Mesozoic granitic magmatism in extensional tectonics near the Mongolian border in China and its implications for crustal growth

Tao Wang[a,*], Yadong Zheng[b], Tianbin Li[c], Yongjun Gao[b]

[a]*Institute of Geology, Chinese Academy of Geological Sciences, Beijing 100037, China*
[b]*Department of Geology, Peking University, Beijing 100871, China*
[c]*Regional Survey Institute of Ningxian Province, Yinchuan 750021, China*

Abstract

The Yagan area of the southernmost Sino–Mongolian border is characterized by an extensional structure where a large metamorphic core complex (Yagan–Onch Hayrhan) and voluminous granitoids are exposed. New isotopic age data indicate that the granitoids, which were previously regarded as Paleozoic in age, were emplaced in early and late Mesozoic times. The early Mesozoic granitoids have 228 ± 7 Ma U–Pb zircon age, and consist of linear mylonitic quartz monzonites and biotite monzogranites. Their chemical compositions are similar to those of potassic granites and shoshonitic series, and show an intraplate and post-collisional environment in tectonic discrimination diagrams. Their fabrics reveal that they experienced syn-emplacement extensional deformation. All these characteristics suggest that the adjustment, thinning and extensional deformation at middle to lower crustal levels might have occurred in the early Mesozoic. The late Mesozoic granitoids have a U–Pb zircon age of 135 ± 2 Ma, and are made up of large elliptical granitic plutons. They are high-K calc-alkaline, and were forcefully emplaced in the dome extensional setting. Both the early and late Mesozoic granitoids have εNd (t) values of -2.3 to $+5$, in strong contrast with the negative εNd (t) values (-11) of the Precambrian host rocks. This suggests that juvenile mantle-derived components were involved in the formation of the granitoids. The similar situation is omnipresent in Central Asia. This study demonstrates that tectonic extension, magmatism and crustal growth are closely related, and that post-collisional and intraplate magmatism was probably a significant process for continental growth in the Phanerozoic.
© 2003 Elsevier Ltd. All rights reserved.

Keywords: Metamorphic core complex; Granitoids; High potassic; U–Pd dating; Central Asian Orogenic Belt

1. Introduction

Mesozoic extensional tectonics is one of the most striking features in the northern and northeastern parts of the North China Block and the south of the Central Asian Orogenic Belt (CAOB). Metamorphic core complexes (MCCs) are typical representatives of extensional tectonics. A large-scale MCC, the Yagan–Onch Hayrhan MCC (simply termed the Yagan MCC in this paper), straddles over the Sino–Mongolian border (Zheng et al., 1991; Zheng and Zhang, 1994; Webb et al., 1999). It reveals that the east-central Asian domain of Mesozoic localized high-strain extension occur in southernmost Mongolia, the hinterland of the Middle-East Asia continent, which is 2500 km continentward of the Pacific margin, and also far from the Mesozoic Mongol–Okhotsk suture in north-east Mongolia.

The dynamics for the high extension has attracted much attention of researchers (e.g. Graham et al., 1996; Johnson et al., 1997; Webb et al., 1997, 1999). Moreover, large contemporaneous granitoids within the MCC have high (near positive) εNd (t) values. Therefore, this provides a good opportunity to study the relationships between typical post-collisional (or orogenic) extension, granitic magmatism and continental crustal growth. This study focuses on the Yagan MCC and its granitoids, showing that the extensional tectonics, granites with high εNd (t) values, and crustal growth are closely associated.

2. Regional geology setting

The study area is located on the southmost Mongolian border in China, and, geologically in the southern margin of the Paleozoic Central Asian Orogenic Belt (CAOB) or Altaids. The Altaid belt to the north and the Manchuride belt (or North China Orogenic belt) to the south are separated by
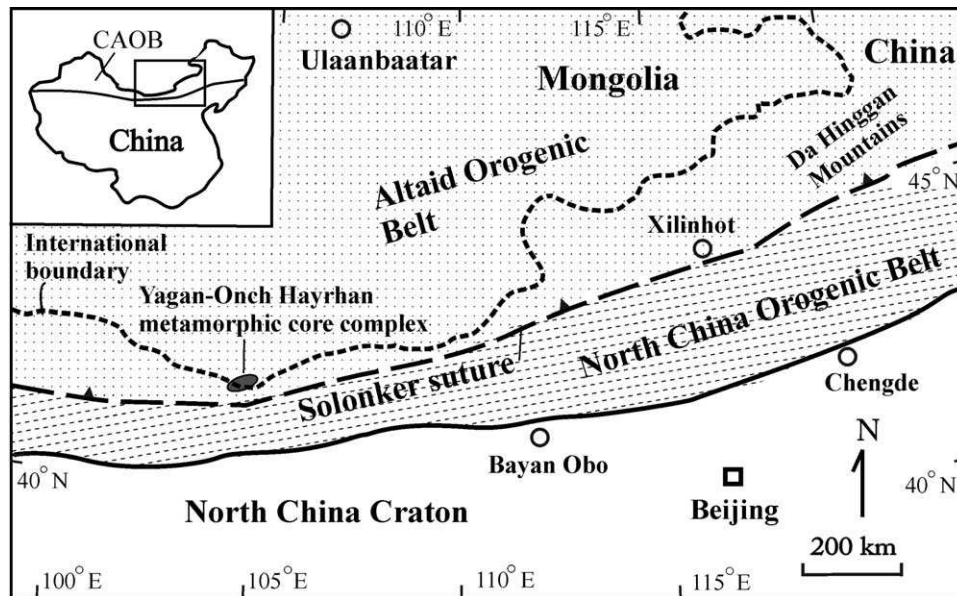
Fig. 1. Tectonic sketch map of the southern part of the Central Asian Orogenic Belt (CAOB) (modified from Sengör and Natal'in, 1996), showing the tectonic setting of the Yagan–Onch Hayrhan metamorphic core complex.

the Solonker suture (Sengör and Natal'in, 1996). The area is located in the north to the suture (Fig. 1).

The area contains high-grade amphibolite-facies metamorphic rocks, Proterozoic weakly metamorphosed shallow marine carbonates locally with stromatolites, Paleozoic weakly metamorphosed rocks and Mesozoic sedimentary rocks. The high-grade metamorphic rocks were regarded as Proterozoic in age (Precambrian basement), and named the 'Gashuilai group' in the Chinese geologic map of the Haribuge area at a scale of 1:200,000 (Ningxia Bureau of Geology, 1982). Also, they were marked as Proterozoic complexes on Mongolia maps of various editions (Yanshin, 1989), and Russian and Mongolian geologists presumed there existed a Proterozoic microcontinent, the South Mongolian microcontinent (Byamba, 1996), including the South Gobi microcontinent (Webb et al., 1999). Recently, Webb et al. (1999) reported Ar–Ar age of 129–126 Ma for biotites from the core metamorphic rocks of the Yagan–Onch Hayrhan MCC and therefore questioned the existence of the South Mongolian microcontinent. However, we obtained a U–Pb zircon age of 916 ± 16 Ma from the gneissic granitoids in the core complex, which indicates that the protolith of the core complex formed before 916 Ma, and provides geochronological evidence for the existence of the South Mongolian microcontinent (Wang et al., 2001a). The Proterozoic weakly metamorphosed shallow marine carbonates are also evidence for the existence of the Proterozoic microcontinent. These Proterozoic carbonates now occur in a thrust slice above the Paleozoic and Mesozoic strata (Zheng et al., 1996).

Permian sedimentary rocks (flysch deposit) are common in the area. They have ENE-trending folds, regional foliation (schistosity or cleavage) and low greenschist facies metamorphism. The rocks and structures were cut

by a granodiorite pluton with 263 ± 2 Ma U–Pb zircon age (Wang, 2000), and covered by unmetamorphosed late Triassic molasses-type terrestrial red beds and conglomerates. The mid-upper Jurassic and low Cretaceous sediments deposited in syn-extensional basins. Associated volcanic rocks have ages ranging from 150 to 130 Ma (e.g. Graham et al., 1996; Webb et al., 1997; Johnson et al., 1997; Webb et al., 1999). Obviously, the contraction tectonic event ended by late Paleozoic times.

3. Extensional tectonics and the Yagan–Onch Hayrhan MCC

Regional extension along the southern margin of the CAOB and the northern margin of the North China Blocks has given rise to several Mesozoic extensional basins (e.g. Ritts et al., 2001) and metamorphic core complexes (MCCs). The Yagan MCC, on the Sino–Mongolian border, is the most typical MCC in China (Zheng and Zhang, 1994). It consists of a lower plate, an upper plate and a master detachment (Fig. 2).

The lower plate, i.e. the crystalline core of the MCC, is made up of Precambrian ($>916 \pm 16$ Ma) amphibolite-facies paragneiss, migmatic gneiss, banded gneiss, marble and quartzite as well as mylonitic granitic plutons (Wang et al., 2001a). Gneissic and mylonitic foliation and stretching lineation are penetrative. The lineation plunges subhorizontally south–southeast, and the shear sense is consistently top-to-southeast, which is the same as that in the detachment zone (Zheng and Zhang, 1994; Webb et al., 1999; Wang, 2000). The footwall rocks grade structurally upwards from low-amphibolite-facies/greenschist facies mylonites into chloritic microbreccias. This suggests that
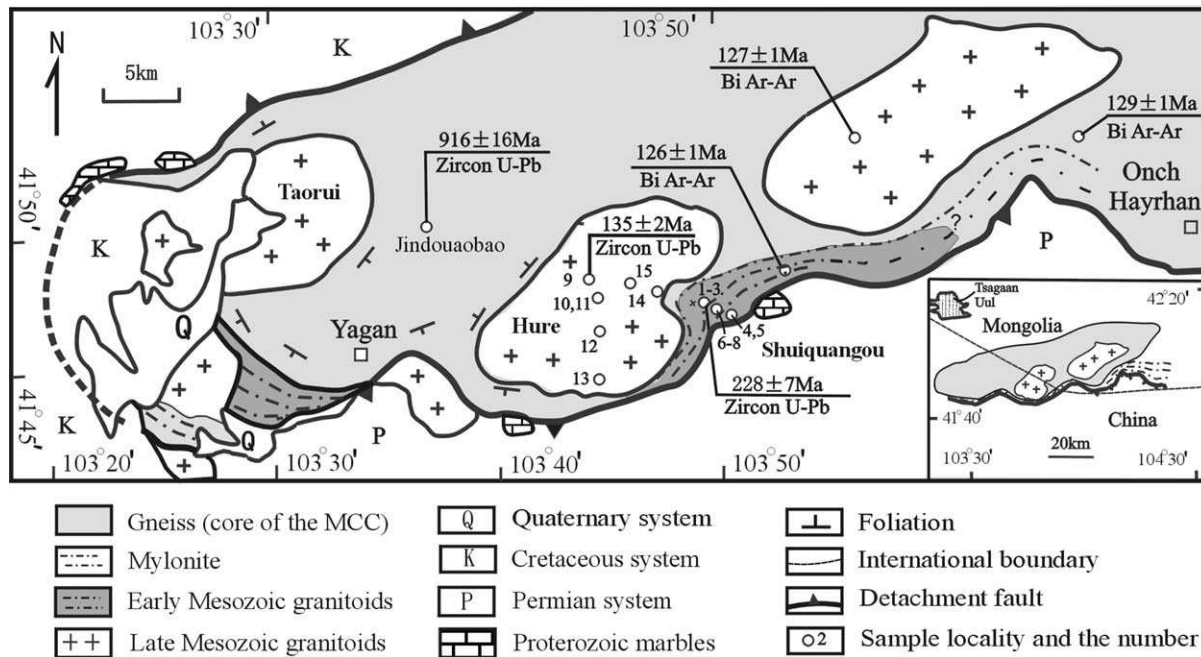
Fig. 2. Geological sketch map of the Yagan–Onch Hayrhan metamorphic core complex. Ar–Ar ages and the inset are after Webb et al. (1999); the inset has been modified according to our mapping in Chinese side. U–Pb ages measured by authors. The number of the samples is sequence number in Table 3.

almost all the rocks of the lower plate underwent progressive extensional shearing. The upper plate includes Permian, Triassic, Jurassic and low Cretaceous rocks. Between the two plates is the master detachment fault containing 5–10 m-thick chloritic microbreccias. Above the microbreccias is a gouge zone and normal fault. All the lineation at different levels has the same plunge (south–southeast or south–southwest) and the shear sense is to-to-the-south (Zheng et al., 2003).

Most published biotite K–Ar, Ar–Ar ages of the mylonites and granitoids range from 155 to 126 Ma (Ningxia Bureau of Geology, 1982; Zheng et al., 1991; Zheng and Zhang, 1994; Webb et al., 1999). These ages, combined with the existence of fragments from the metamorphic cores of the Jurassic and Cretaceous syn-extensional basins, imply that the development of the Yagan MCC commenced at least in the early Jurassic and continued until the late Cretaceous. Our new isotopic age data, however, reveal that the early deep-levels extensional deformation, recorded in the high-grade metamorphic core rocks, started much earlier (Wang, 2000, see below).

4. Mesozoic granitic magmatism in the MCC

Granitic plutons occupy nearly 40–50% of the area of the core of the Yagan MCC. As they are located in the Paleozoic orogenic belt, almost all were marked as Paleozoic magmatic rocks on Chinese and Mongolia geological maps, and they were considered as a part of the Paleozoic orogenic belt. Our new isotopic age data,

however, indicate that they were emplaced during Mesozoic times: early and late Mesozoic, respectively.

4.1. Early Mesozoic granitoids

4.1.1. Occurrence, deformation and petrology

The early Mesozoic granitoids have been strongly deformed (mylonitized). They occur in small linear-shape mylonitic granitic plutons, parallel to the regional exten-sional shear foliation, and occupy 10–20% of the core of the MCC. The rock types are mainly mylonitic porphyritic quartz monzonites and porphyritic monzogranites. Most of them have a mylonitic texture. The porphyroclasts (about 30–45%) consist of K-feldspar (25–30%) and plagioclase (15–20%), and the matrix (55–60%) of quartz (15–25%), feldspar (30–40%) and biotite (5% ±).

The Shuiquangou pluton is the largest and the most typical. It occurs below the detachment fault (Fig. 2), and contains a pervasive foliation and stretching or mineral lineation. The rock fabrics are typically S–L, and most L > S type, and were successively formed during magmatic flow, high temperature solid-state flow and middle–low temperature solid-state flow (Wang et al., 2001b), showing a down-temperature solid-state deformation process (Tribe and D'lemos, 1996), which is a characteristic of syn-tectonic granites. The subunits of the pluton show the same attitude of the foliation and lineation and have the same strain types, although they are different in deformation intensity. All most shear sense indicators indicate consist (top-to-southeast) shear deformation, similar to the regional extensional shear (Zheng et al., 1991; Zheng and Zhang,

Table 1
U–Pb isotopic data and age for the early Mesozoic granitoids

Grain type	Grain wt. (μg)	Pb_c (pg)	U (ppm)	Isotope ratios						Apparent ages (Ma)		
				$^{206}Pb_m/^{204}Pb$	$^{206}Pb_c/^{208}Pb$	$^{206}Pb^*/^{238}U$	$2\sigma m$	$^{207}Pb^*/^{235}U$	$2\sigma m$	$^{206}Pb^*/^{238}U$	$^{207}Pb^*/^{235}U$	$^{207}Pb^*/^{206}Pb^*$
8*A*	25	17	599	1895	5.0	0.03346	66	0.23452	122	212.2 ± 1.4	213.9 ± 2.4	233 ± 19
6*B*	36	365	2405	510	3.8	0.03265	94	0.23436	378	207.1 ± 1.9	213.8 ± 7.1	287 ± 71
5*C*	51	465	1458	326	3.9	0.03040	66	0.21413	313	193.0 ± 1.3	197.0 ± 5.5	245 ± 60
4*D*	73	28	441	2620	4.9	0.03608	42	0.25216	87	228.5 ± 0.9	228.3 ± 1.8	227 ± 15
1*E*a	25	7	656	5440	6.0	0.03619	52	0.25340	88	229.2 ± 1.2	229.3 ± 1.8	231 ± 13
1*E*a	28	6	978	1055	3.6	0.03565	158	0.24712	212	225.8 ± 3.6	224.2 ± 4.2	208 ± 25
1*E*a	31	26	709	1948	5.4	0.03573	50	0.25045	111	226.3 ± 1.1	226.9 ± 2.3	234 ± 20

Notes: Grain type: $A = \sim 100\mu$, $B = \sim 120\mu$, $C = \sim 140\mu$, $D = \sim 170\mu$, $E = \sim 200\mu$, a = abraded in air abrasion device. Number refers to number of grains analyzed. * = radiogenic Pb. $^{206}Pb/^{204}Pb$ is measured ratio, uncorrected for blank, spike, or fractionation. $^{206}Pb/^{208}Pb$ is corrected for blank, spike, and fractionation. Analyzed in the laboratory of the Department of Geology, University of Arizona, Tucson, Arizona, U.S.A (see Appendix A).

1994). This suggests that they underwent the same progressive extensional shear deformation.

4.1.2. Zircon U–Pb dating

The mylonitic biotite–quartz monzonites are the earliest unit of the early Mesozoic mylonitic granitoids. They were dated to constrain the age of the earliest magmatism. The samples were collected in the Shuiquanguo pluton (Fig. 2) and were processed for heavy minerals. 1.3 g of colorless to very light-tan zircon grains up to 250 μm long were extracted. The grains are all very similar in shape, and have well-formed crystal faces and pyramidal terminations. No cores were observed. The U–Pb analyses were made by G.E. Gehrels in the laboratory of the Department of Geology, University of Arizona, Tucson, Arizona, USA. The results (Table 1 and Fig. 3) show that five data points produce a good discordant line, yielding an upper intercept age of 228 ± 7 Ma with MSWD = 1.07. The age is interpreted as the crystallization age of the zircon, representing the earliest time of pluton emplacement.

4.2. Late Mesozoic granitoids

4.2.1. Occurrence, deformation and petrology

The late Mesozoic granite plutons are dominant and occupy 30–40% of the core of the MCC. They consist of larger elliptical or irregular elliptical plutons, such as Hure and Taorui plutons in China, and cut the early Mesozoic granitoid plutons, demonstrating a clear age relationships (Fig. 2).

The plutons mainly consist of two units. The first is medium to fine-grained gray-white biotite granodiorite, and occurs in the margins of the plutons. Major minerals are plagioclase (25–35%), K-feldspar (30–40%), quartz (25–30%) and biotite (1–5%). The second unit in the center constitutes the major part of the plutons. Its rock type is biotite monzogranite with inequant K-feldspar phenocrysts, and constituent minerals are plagioclase (15–25%), K-feldspar (35–45%), quartz (25–33%) and biotite (1–5%).

Both units have the same accessory zircon, apatite, magnetite and sphene.

The distribution of the two units defines a concentric shape. Foliation occurs at the margins of the plutons and no (or very weak) foliation in the centers, showing higher strain at the margins and no (or even lower) strain in the center. Additionally, the wall rocks near the pluton have been deformed, characterized by folds of the regional foliation. These are features of forcefully emplaced ballooning plutons. This process provided about 16–24% space of the present volume of the plutons (Wang et al., 2002), estimated by host-rock ductile shortening (Wang et al., 2000). This suggests that forceful emplacement did occur in an extensional setting.

4.2.2. Enclaves

Dark, elliptical or irregular-shaped enclaves occasionally occur in the granitoids. Their textures are characteristic of
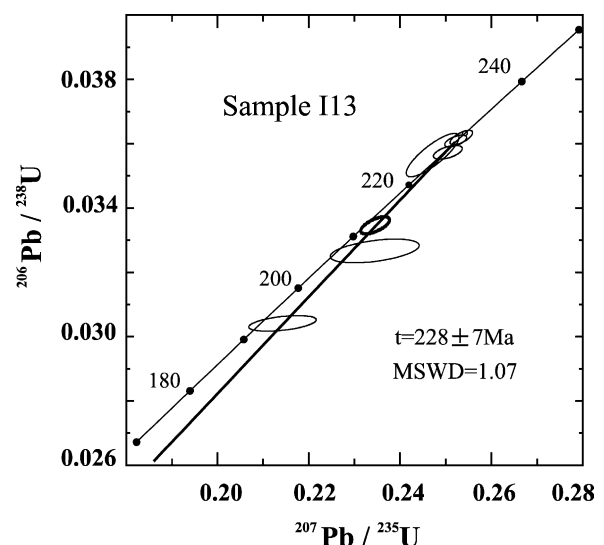

Fig. 3. Concordia diagram for U–Pb zircon age for the early Mesozoic mylonitic granitoids (Shuiquangou pluton), analyzed in the laboratory of the Department of Geology, University of Arizona, Tucson, Arizona, U.S.A.

Table 2
U–Pb isotopic data and age for the late Mesozoic granitoids

Grain						Isotope ratios								Apparent ages (Ma)		
No	Wt. (μg)	Pb (pg)	U (ppm)	Pb_c	$^{206}Pb_c/^{208}Pb$	$^{206}Pb_m/^{204}Pb$	$^{206}Pb/^{238}U$	$2\sigma m$	$^{207}Pb/^{235}U$	$2\sigma m$	$^{207}Pb/^{206}Pb$	$2\sigma m$	$^{206}Pb/^{238}U$	$^{207}Pb/^{235}U$	$^{207}Pb/^{206}Pb$
1	5	68	3159	0.093	10.0	191	0.01597	29	0.1050	33	0.04770	144	102.2	101.4	84.2
2	10	55	2695	0.110	7.7	271	0.01626	8	0.1073	8	0.04788	27	104.0	103.5	93.1
3	10	56	2226	0.200	6.3	129	0.15530	14	0.1053	17	0.04918	58	99.3	101.7	156.2
4	15	22	910	0.075	7.1	236	0.01871	34	0.1245	37	0.04827	103	119.5	119.2	112.4
5	10	152	5513	0.400	10.9	199	0.02073	12	0.1391	14	0.04867	36	132.3	132.3	131.8
6	10	19	764	0.032	16.1	336	0.02117	27	0.1420	3	0.04864	76	135.1	134.8	130.4

Notes: Grain:1—yellow semitransparent stubby; 2—yellow semitransparent acicular; 3—light-yellow transparent acicular; 4—light-yellow transparent long prisms; 5—yellow semitransparent stubby; 6—yellow semitransparent long prisms. Analyzed at the Tianjin Institute of Geology and Mineral Resources, China Geological Survey (see Appendix A).

magmatic crystallization. Two kinds of enclaves are recognized. One is biotites quartz diorite with biotite (15–20%), plagioclase (60–70%), K-feldspar (5–10%) and quartz (10–15%). The other is quartz monzonite containing biotite (10–15%), plagioclase (25–30%), K-feldspar (40–45%) and quartz (8–12%).

4.2.3. Zircon U–Pb dating

The samples were taken from a biotite monzogranite of the second unit in the center of the Hure pluton (Fig. 2). The zircon grains have well-formed crystal faces and pyramidal terminations of magmatic origin. The U–Pb isotopic dating was done by Prof. Hui-min Li in the U–Pb isotope laboratory of the Geological Institute of Tianjing, China. The analytical methods and processes were described in detail by Li et al. (1995). The zircon grains are slightly different in shape and were analyzed separately. The analyses yielded three groups of ages: 104 ± 1 Ma (grains No. 1 and 2), 120 ± 2 Ma (No. 4) and 135 ± 2 Ma (No. 5, 6) (Table 2, Fig. 4). The discordant line consisting of the grains of No. 3, 4, 5 and 6 yields an upper intercept age of 131 ± 11 Ma and a lower intercept age of -77 ± 104 Ma with MSWD = 0.57. As the zircon grains are relatively young, a precise $^{206}Pb/^{208}U$ apparent age would be preferable. The $^{206}Pb/^{208}U$ apparent age of 135 ± 2 Ma of the zircon grain No. 6, similar to the age of the third group, may represent the earliest intrusion age of the pluton. It is also comparable with the age of the upper incept age of 131 ± 11 Ma, and with the statistic mean apparent age of 133 ± 1 Ma of grains of No 5 and 6. The ages of 104 ± 1 and 120 ± 2 Ma may be influenced by later thermal events. The age of 135 ± 2 Ma is almost the same as a biotite Ar–Ar age of 135 Ma for the Hure pluton reported by Zheng and Zhang (1994). Webb et al. (1999) also determined a biotite Ar–Ar age of 127 Ma for a large pluton near the Hure
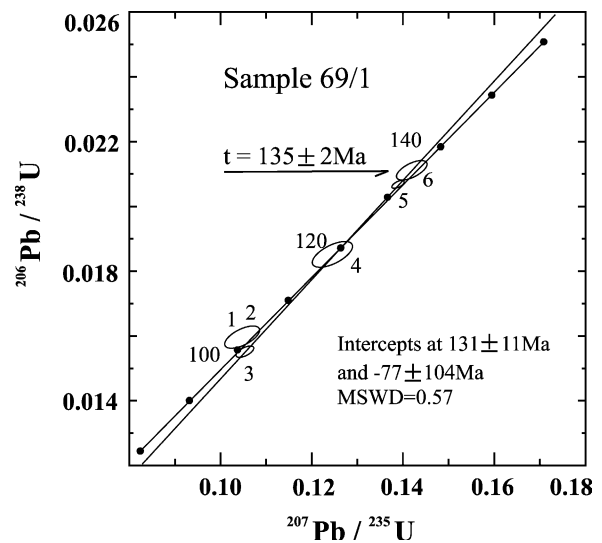

Fig. 4. Concordia diagram for U–Pb zircon age of the late Mesozoic granitoids (Hure pluton), analyzed at the Tianjin Institute of Geology and Mineral Resources, China Geological Survey.

Table 3
Major and trace element compositions of the Mesozoic granitoids

Pluton No	Early Mesozoic granitoids								Late Mesozoic granitoids						
	1 (I9)	2 (113)	3 (N7)	4 (31)	5 (18)	6 (179/1)	7 (007/1)	8 (I32)	9 (069/1)	10 (071/1)	11 (071/3)	12 (073/1)	13 (075/2)	14 (154/1)	15 (156/1)
SiO_2	64.11	64.31	65.14	55.09	61.22	63.40	72.83	75.91	73.90	73.57	59.57	69.65	74.96	74.59	69.92
TiO_2	0.32	0.56	0.47	0.65	0.36	0.36	0.18	0.06	0.15	0.19	1.52	0.41	0.08	0.15	0.46
Al_2O_3	16.88	16.53	16.75	19.72	18.27	18.12	13.84	13.44	13.45	13.00	14.25	14.97	13.25	13.23	14.60
Fe_2O_3	0.79	2.02	1.03	3.24	2.02	2.46	0.75	0.09	0.40	0.26	2.20	0.80	0.09	0.50	0.63
FeO	1.13	1.99	1.68	2.93	1.24	0.23	0.70	0.29	1.04	1.49	6.50	1.45	0.56	0.70	1.49
MnO	0.13	0.14	0.12	0.15	0.08	0.03	0.03	0.09	0.07	0.06	0.20	0.08	0.06	0.06	0.11
MgO	0.50	1.21	0.76	2.55	0.79	0.49	0.24	0.09	0.34	0.66	3.64	0.81	0.31	0.56	0.86
CaO	2.17	2.08	2.02	3.53	2.14	0.70	1.08	0.09	1.32	1.37	1.51	2.25	0.86	1.09	1.74
Na_2O	3.95	5.05	4.93	5.02	6.21	5.89	3.48	3.91	4.03	3.42	2.53	4.28	4.02	4.13	4.28
K_2O	8.22	5.69	6.76	5.29	5.87	6.89	5.95	4.71	4.81	5.65	6.62	3.96	4.88	4.95	4.59
P_2O_5	0.14	0.32	0.17	0.79	0.25	0.15	0.04	0.01	0.05	0.13	0.38	0.14	0.03	0.07	0.16
H_2O^+	0.56	0.24	0.34	0.78	0.62	0.48	0.42	0.50	0.30	0.42	1.18	0.48	0.24	0.26	0.42
Los	1.02	0.37	0.54	0.80	1.31	0.68	0.47	0.64	0.34	0.47	0.84	0.91	0.24	0.28	0.27
Total	99.92	100.51	100.71	100.54	100.38	99.88	100.01	99.83	100.20	100.69	100.94	100.19	99.58	100.57	99.53
A/NK	1.10	1.14	1.09	1.41	1.10	1.06	1.14	1.17	1.14	1.11	1.26	1.32	1.11	1.09	1.22
A/NCK	0.87	0.91	0.88	0.97	0.89	0.98	0.98	1.15	0.95	0.91	1.01	0.97	0.98	0.94	0.96
δ	7.02	5.41	6.17	8.79	8.01	8.01	2.98	2.26	2.53	2.69	5.05	2.55	2.48	2.61	2.92
W	0.41	0.50	0.38	0.53	0.62	0.91	0.52	0.24	0.28	0.15	0.25	0.36	0.14	0.42	0.30
Cr	7.3	5	6	16	14	12	14	14	24	21	22	13	9	18	13
Co	1.7	27	25	12	2.9	1.4	0.1	0.1	5	5	16	8	62	5	59
Ni	4	5	4.2	6.7	4.0	4.1	4	4	10	5	5	5	5	16	7
V	10.2	29	27	92	25	24	1.5	1.5	7	11	159	31	5	5	30
Th	13	10	11	35	14	30	104	21	38	64	10	20	9	23	22
Rb	384	273	251	238	207	209	172	337	239	314	534	126	384	336	281
Sr	742.7	1044	984	3890	1360	770	82	235	131	84	257	588	123	89	243
Ba	1275	1122	1234	2670	1600	1110	246	170	242	242	1557	899	261	249	863
Ta	2.3	3	3.8	2.4	1.8	3.3	0.2	1.8	0.5	0.8	1.0	1.7	1.3	0.8	1.4
Nb	43	36	42	35.0	15	43	8	24	6	12	8	2	12	12	25
Hf	2.3	2	2.6	1.5	1.9	4.6	1.7	2.1	1.9	2.7	10	1.6	1.4	2.3	2.2
Zr	84.2	581	476	78.0	69	174	105	38	101	158	271	181	12	84	231
Ga	26	26	27	32.0	26	29	13	33	22	22	31	22	25	21	24
U	2.5	5	3.2	5.5	2.7	4	4.2	2.4	5	5	5	5	5	5	5
La	90.38	133.9	128.65	185.3	69.59	125.7	69.28	4.79	25.46	58.75	26.33	34.80	11.2	24.49	43.5
Ce	200.3	252.0	231.4	298.6	105.2	235.0	127.5	5.72	44.82	102.10	45.92	53.40	20.2	43.29	69.61
Pr	19.51	25.78	24.15	27.73	9.39	22.37	11.67	0.74	3.96	9.88	4.63	4.99	2.39	4.04	7.34
Nd	73.41	101.6	90.65	96.74	32.31	78.66	39.39	3.33	18.06	37.07	18.56	17.01	8.79	16.64	27.65
Sm	11.26	15.99	14.81	12.95	4.10	11.55	6.45	1.02	4.58	6.49	3.88	2.17	2.49	3.63	5.67
Eu	2.09	2.77	2.67	2.96	1.48	2.14	0.57	0.41	0.44	0.59	0.58	0.51	0.27	0.33	0.60
Gd	9.59	15.20	14.32	12.01	3.24	10.64	4.79	1.92	6.17	4.57	4.38	1.96	2.24	4.94	6.36
Tb	1.12	1.67	1.47	1.41	0.39	1.40	0.42	0.42	1.04	0.32	0.47	0.30	0.32	0.67	0.93
Dy	6.09	9.36	7.38	5.37	1.51	6.26	1.48	3.26	7.22	2.08	2.50	0.92	2.11	4.25	4.53
Ho	1.11	1.84	1.74	0.94	0.28	1.13	0.21	0.79	1.53	0.30	0.45	0.19	0.39	0.77	0.78
Er	3.14	4.74	4.47	2.83	0.73	3.15	0.60	2.63	4.07	0.73	1.27	0.53	0.92	2.28	1.94
Tm	0.42	0.68	0.57	0.36	0.10	0.41	0.10	0.41	0.60	0.10	0.19	0.10	0.14	0.33	0.30
Yb	2.18	4.29	4.03	2.06	0.49	2.71	0.23	3.62	3.40	0.46	1.20	0.41	1.09	2.13	1.71
Lu	0.23	0.67	0.57	0.34	0.10	0.41	0.10	0.61	0.63	0.10	0.17	0.10	0.22	0.34	0.26
Y	26.04	45.49	39.74	22.83	5.28	28.54	3.34	22.74	43.35	7.03	13.47	3.67	10.49	23.17	19.58
δEu	0.60	0.53	0.59	0.71	1.20	0.58	0.30	0.88	0.25	0.31	0.43	0.74	0.34	0.24	0.30
$(La/Yb)_N$	28.02	21.09	20.41	60.78	95.97	31.34	203.55	0.89	5.06	86.30	14.83	57.36	6.94	7.77	17.19
Ta/Yb	1.06	0.70	0.94	1.17	3.67	1.22	0.87	0.50	0.15	1.74	0.83	4.15	1.19	0.38	0.82
Ce/Yb	92	59	57	145	215	87	554	2	13	222	38	130	19	20	41

1,2,3,5—mylonitic biotite-quartz monzonite; 4—gneissic quartz diorite; 6—mylonitic biotite monzogranite; 7—monzogranite; 8—garnet granite; 9,11,12,13—biotite monzogranite;10—biotite granodiorite; 14—diorite enclave; 15—monzonite enclave. A/CNK = mol $Al_2O_3/(Na_2O + K_2O + CaO)$; A/NK = molar $(Al_2O3/Na_2O + K_2O)$; δ = molar $(Na_2O + K_2O)/(Si_2O\text{-}43)$. W = $Fe_2O_3/(FeO + Fe_2O_3)$.

Table 4
Sr and Nd isotopic data for the Mesozoic granitoid from the Yagan MCC

Sample No.	Rock type	Rb (ppm)	Sr (ppm)	$^{87}Rb/^{86}Sr$	$^{87}Sr/^{86}Sr$	$2\sigma m$	I_{Sr}	Sm (ppm)	Nd (ppm)	$^{147}Sm/^{144}Nd$	$^{143}Nd/^{144}Nd$	$2\sigma m$	$\varepsilon_{Nd}(0)$	$f_{Sm/Nd}$	$\varepsilon_{Nd}(t)$	T_{DM}(Ga)
Late Mesozoic grantoids						(135 Ma)						(present)		(135 Ma)		
071/1	Bi-granodiorite	30.9	84.3	10.60	0.733806	14	0.71347	7.38	41.57	0.1073	0.5124800	8	−3.1	−0.45	−1.5	0.96
069/1	Bi-Monzonite	221.5	133.1	4.82	0.716223	17	0.70698	3.24	13.73	0.1429	0.5128550	35	4.2	−0.27	5.2	0.64
075/2	Bi-monzogranite	350.2	123.4	8.22	0.72661	14	0.71085	3.13	11.77	0.1609	0.5126340	14	−0.1	−0.18	0.5	1.49
073/1	Enclave	109.0	676.3	0.467	0.706324	17	0.70543	2.60	19.13	0.0822	0.5125980	9	−0.8	−0.58	1.2	0.64
Early Mesozoic granites						(228 Ma)								(228 Ma)		
I32	Garnet monzogranite	306.8	227.2	3.90	0.715570	12	0.70292	1.66	5.77	0.1740	0.5125620	11	−1.5	−0.12	−0.8	2.25
I09	Q-monzonite	393.8	1193.0	0.95	0.709727	14	0.70664	12.52	73.22	0.1034	0.5123850	7	−4.9	−0.47	−2.2	1.06
N07	Q-Monzonite	329.7	773.7	1.23	0.710795	15	0.70680	17.38	108.00	0.0974	0.5123840	7	−5.0	−0.50	−2.1	1.00
7	Bi-Monzogranite	332.9	83.0	11.61	0.734215	15	0.69657	7.65	44.58	0.1037	0.5123810	9	−5.0	−0.47	−2.3	1.07
I13	Q-monzonite	263.9	1011.0	0.756	0.709764	9	0.70731	17.23	106.58	0.0978	0.5124220	7	−4.2	−0.50	−1.3	0.96
Gneisses (Precambrian besement)						(135 Ma)								(135 Ma)		
084/3	Bi-Pl-gneisses	101.2	309.4	0.947	0.736052	18	0.73423	4.80	24.28	0.1195	0.5120140	17	−12.2	−0.39	−10.8	1.83

Note: $\varepsilon_{Nd} = ((^{143}Nd/^{144}Nd)_s/(^{143}Nd/^{144}Nd)_{CHUR} - 1) \times 10000$, $f_{Sm/Nd} = (^{147}Sm/^{144}Nd)_s/(^{147}Sm/^{144}Nd)_{CHUR} - 1$, where s = sample, $(^{143}Nd/^{144}Nd)_{CHUR} = 0.512638$, and $(^{147}Sm/^{144}Nd)_{CHUR} = 0.1966$. The model ages ($T_{DM}$) were calculated using a linear isotopic ratio growth equation: $T_{DM} = 1/\lambda \times \ln(1 + ((^{143}Nd/^{144}Nd)_s - 0.51315)/((^{147}Sm/^{144}Nd)_s - 0.2137))$. Bi, Q, Pl are biotite, quartz and plagioclase, respectively.

pluton, both of which belongs to the same suit (Fig. 2). In any case, the available age data indicate a rapid cooling history.

5. Geochemistry of the granitoids

Granitoid samples of the Mesozoic granitoids were analyzed for their major, trace elements (Table 3) and for Sr and Nd isotopic compositions (Table 4). Some observations can be made as follows.

5.1. Major elements

The early Mesozoic granitoids have low SiO_2 (mostly 55–65%) and high Al_2O_3 (mostly 16–19%), K_2O (5.3–8.2%), Na_2O (4–6%) and FeO_t (2–5%). Their A/CNK (= mol Al_2O_3/($Na_2O + K_2O + CaO$)) mostly range from 0.89 to 0.98 and A/NK (= molar Al_2O_3/($Na_2O + K_2O$)) are always larger than 1, indicating metaluminous composition (Table 3, Fig. 5a). Their δ Index ($Na_2O + K_2O$)/(Si_2O-43) ranges from 2.98 to 8.01 and mostly >4, demonstrating alkalic features. In major element discrimination diagrams, the analyzed samples fall in the fields of alkaline granite and A-type granite (e.g. Fig. 5b). A striking characteristic is that they are highly enriched in K_2O (4.7–8.3%) (Fig. 5c), and their K_2O/Na_2O ratios are mostly in range 0.95–2.08 and few >2(much higher than 0.5). This is a feature of shoshonitic series (Peccerillo and Taylor, 1976; Väisänen et al., 2000) or even super-shoshonitic series (K_2O/Na_2O >2) (Turner et al., 1996).

The late Mesozoic granitoids are relatively homogeneous in composition. They have higher SiO_2 (69–79%) and lower Al_2O_3 (13–15%), K_2O (4.6–5.7%) and Na_2O (3.4–4.3%), in comparison with the early Mesozoic granitoids. Their A/CNK values (0.94–1.31) are slightly higher than those of the early Mesozoic granitoids, and the data points straddle the boundary between metaluminous and peraluminous (Fig. 5a). They are mostly constrained to the I- or S-type granite fields in Fig. 5b. Their K_2O content (4.59–6.62%) and K_2O/Na_2O ratios (0.93–1.65) are lower than those of the early Mesozoic granitoids, and the samples mainly fall in the high-K calc-alkaline field (Fig. 5c). All these characteristics indicate the late Mesozoic granitoids are high-K calc-alkaline granites.

5.2. Trace elements

The trace element contents are represented in primitive mantle-normalized diagrams or spidergrams (Fig. 6), and REE contents in chondrite-normalized diagrams (Fig. 7).

The early Mesozoic granitoids are relatively enriched in LILE such as Rb, Ba, Sr, and some HFSE such as Nd, Th, Y, and show negative anomalies of Nb P, Zr and Ti in the spidergram (Fig. 6). They share same position as potassic granitoids of East Africa (Küster and Harms, 1998) in
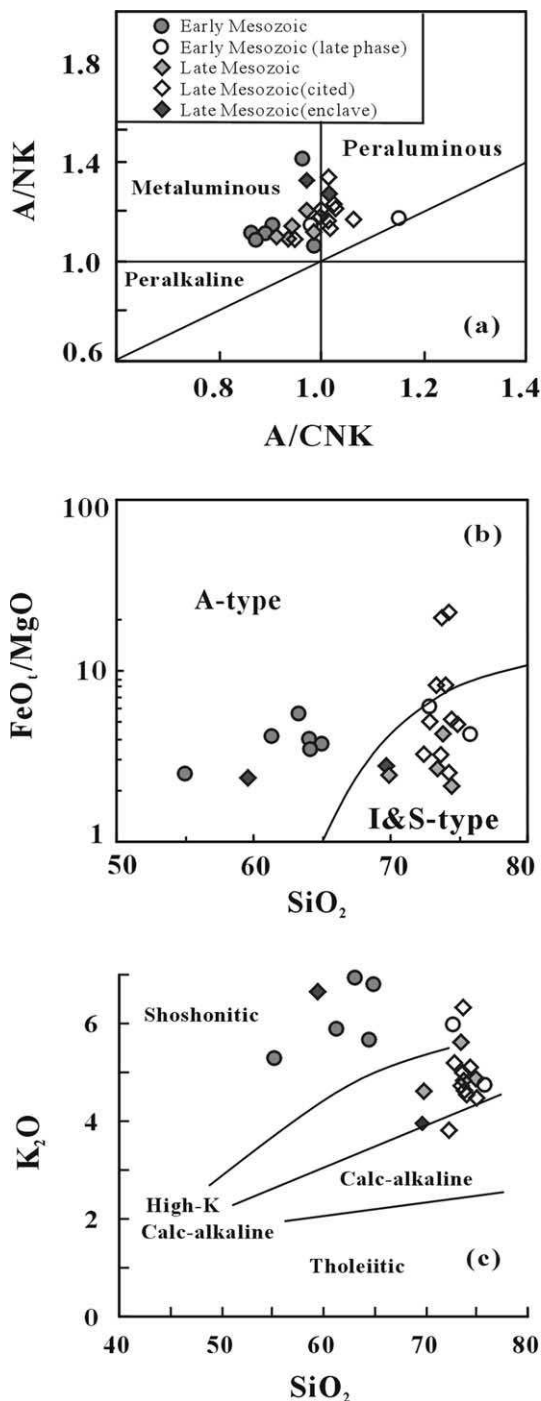
Fig. 5. Major element diagrams for rock types of the Mesozoic granitoids from the Yagan MCC. (a) A/CNK vs. A/NK diagram (Shand's molar parameters in the diagram of Maniar and Piccoli, 1989), A/CNK = mol $Al_2O_3/(Na_2O + K_2O + CaO)$, A/NK = molar $Al_2O/(Na_2O + K_2O)$; (b) SiO_2 vs. FeO_t/MgO diagram (after Whalen et al., 1987); (c) SiO_2 vs. K_2O-diagram (boundary after Peccerillo and Taylor, 1976). The data cited from Ningxia Bureau of Geology (1982).

diagrams of $Zr + Nb + Ce + Y–FeO_t/MgO$ and $Rb–(Nb + Y)$, and their ratios of Ce/Yb are larger than 20, displaying potassic or even shoshonitic nature (Pearce, 1982). In some discrimination diagrams for A-type granites,
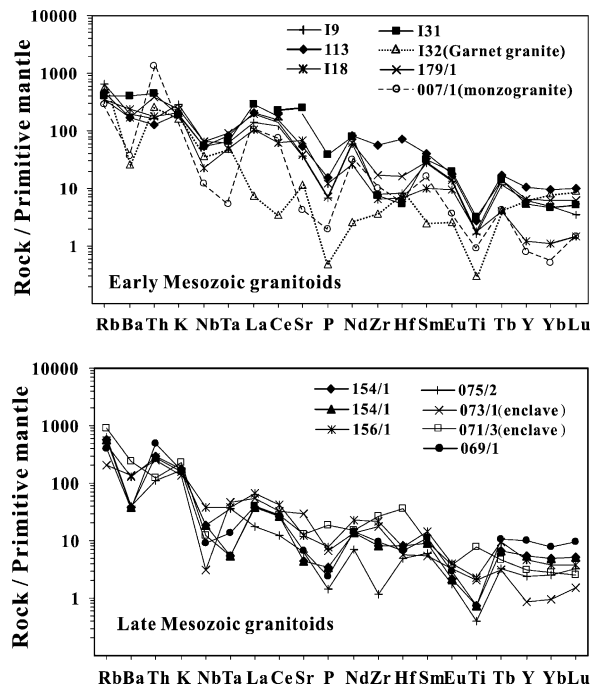
Fig. 6. Primitive mantle-normalized spidergrams for the Mesozoic granitoids of the Yagan MCC, using the normalization value of Sun and McDonough (1989).

the samples fall in the A-type field or on the borders of I (or S)- type and A-type field (e.g. Fig. 8). However, they are different from typical A-type granitoids in many aspects. Their Al_2O_3 ($>13\%$) is higher and A/NCK is mostly >0.91 (Al_2O_3 of typical A-type granitoids is generally $<12\%$,
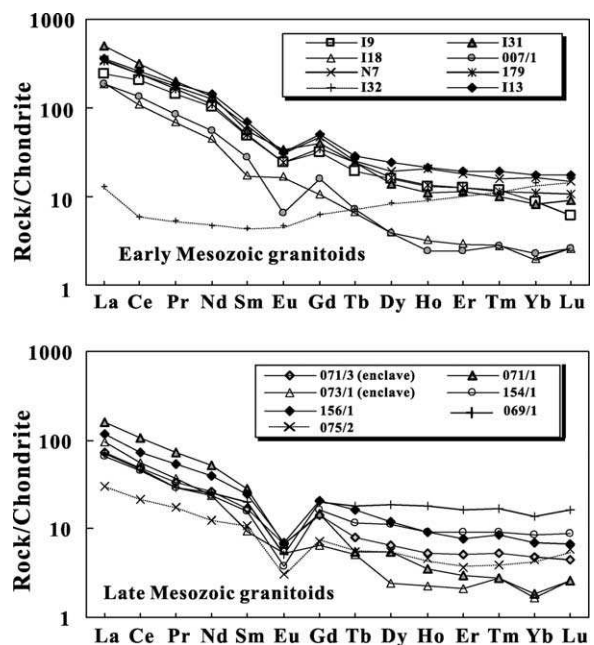
Fig. 7. Chondrite-normalized REE patterns for the Mesozoic granitoids of the Yagan MCC, using the normalization value of Sun and McDonough (1989).
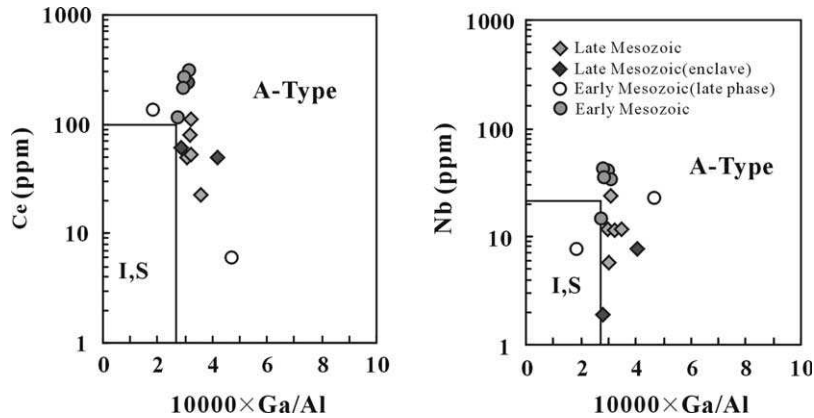
Fig. 8. Plots of the Mesozoic granitoids in discrimination diagrams for A-type granitoids. Ce, Nd content vs. 10,000 × Ga/Al correlation diagram (Whalen et al., 1987). I, S = field for I and S-type granitoids.

A/NCK < 0.95) (Table 3). The contents of Fe_2O_3, Ti, P and W value (Fe_2O_3/(FeO + Fe_2O_3)) are low (Table 3). Additionally, their REE patterns also do not show the nature of A-type granites. The patterns show slightly negative Eu anomalies (Eu/Eu* = 0.30–1.20), rather than a strong negative Eu anomalies as most typical alkaline granites do. The REE are high in abundances, particularly in light REE (LREE) abundances, and the REE patterns display fraction with (La/Yb)$_N$ ratios ranging from 20 to 60. As to the garnet granites (sample I32), its unusual REE pattern may be due to their relative high-contents of garnet.

The late Mesozoic granitoids have trace elements and REE patterns roughly similar to those of the early Mesozoic granitoids (Figs. 6 and 7). Ba, Sr, Nb, Eu, and Ti negative anomalies are also pronounced (Fig. 6). However, the rocks are more enriched in Rb and depleted in Nb, Ta. For example, the Nb content (2–12 ppm) of most samples (except No 156/1) is lower than that of the early Mesozoic granitoids. Compared with the early Mesozoic granitoids, the late Mesozoic granitoids have relatively lower REE abundances (Fig. 7), and lower (La/Yb)$_N$ ratios (mainly ranging from 5 to 57).

However, they exhibit more pronounced negative Eu anomalies (Eu/Eu* = 0.24–0.74).

In various discrimination diagrams, most samples of the late Mesozoic granitoids plot in the I/S-type field (e. g. Fig. 5c) and in the boundary area with A-type granites (Fig. 8). The 10000 × Ga/Al ratios are from 2.78 to 4.11 with a sharp value in 3.10–3.30, which are significantly higher than those of I-type and S-type granitoids, but lower than the average value of 3.75 for A-type granites (Whalen et al, 1987). One enclave sample (No. 71/3) (biotite quartz diorite) shows some similarities with shoshonitic and alkaline granites, similar to the early Mesozoic granitoids. In contrast, another enclave sample (73/1) is typical of calc-alkaline granites (Fig. 5b and c).

In various tectonic setting discrimination diagrams, most samples of the early Mesozoic granitoids fall in the fields of intraplate or post-collision, and they are the only group that falls in the field of intraplate tectonic setting (Fig. 9a and b). Compared with the other granitoids in the Yagan MCC (Wang, 2000), they are more comparable to granitoids formed in an extensional tectonic setting. The late Mesozoic granitoids, however, show different tectonic environments
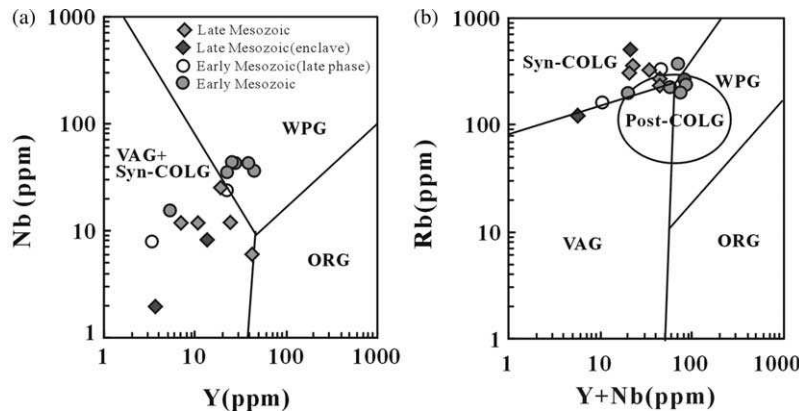

Fig. 9. Tectonic setting discrimination for the granitoids in the Yagan MCC. Y–Nd diagram after Pearce et al., (1984); Rb–Y + Nb diagram after Pearce (1996); Pre-, Syn- and Post-CLOG-pre-, syn- and post-collisional granites, respectively; VAG—volcanic-arc granites, WPG—within-plate granites, ORG—ocean ridge granites.

in different tectonic discrimination diagrams. For example, they plot in the volcanic arc field and syn-collision in field in Fig. 9a and b, and in the post-orogenic field in a R1–R2 diagram (Batchelor and Bowden, 1985). Such ambiguities are typical for post-collisional granitoids in general (cf. Pearce, 1996). In fact, the late Mesozoic granitoids were emplaced during the formation of the Yagan MCC, i.e. in a post-orogenic extensional setting (Wang et al., 2002), as to be discussed later.

5.3. Isotopic compositions

Sr and Nd isotope data for both the early and late Mesozoic granitoids are summarized in Table 4.

The early Mesozoic granitoids have a narrow range of εNd (t) values (-2 to -1), and the model ages (T_{DM}) mostly range from 0.96 to 1.07 Ma. Their (^{87}Sr/^{86}Sr)i values are mainly between 0.7066 and 0.7079 (Fig. 10). The (^{87}Sr/^{86}Sr)i value of sample 7/1 may have no petrogenetic significance, because it shows unrealistic low (^{87}Sr/^{86}Sr)i values (0.69657) which is probably caused by high Rb/Sr ratio (Jahn et al., 2000a).

The late Mesozoic granitoids show highly variable (^{87}Sr/^{86}Sr)i ratios ranging from 0.705 to 0.713. Their εNd (t) values are slightly positive (0 to $+0.5$), except for sample 7/1 (-1.54), and the model ages (T_{DM}) are mainly between 0.64 and 1.49 Ga, younger than those of the early Mesozoic granitoids. The (^{87}Sr/^{86}Sr)i ratios (0.7054), εNd (t) values ($+1.2$) and their model ages (T_{DM}) (0.64 Ga) of the enclaves within them were approximately estimated by the age (135 Ma) of their host rocks. These features are similar to those of their host rocks. As isotopic data of Nd are known
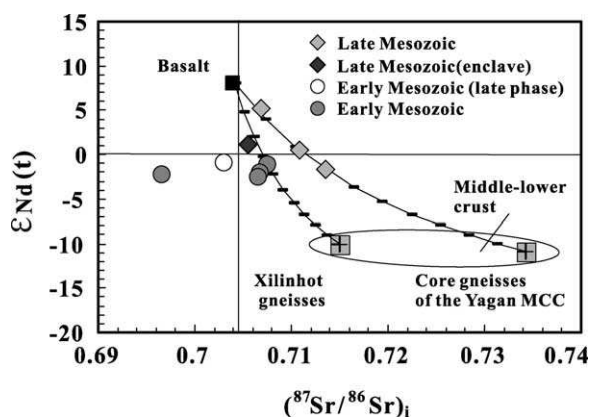
Fig. 10. εNd (t) vs. ^{87}Sr/^{86}Sr (t) diagram for the granitoids (the early and late Mesozoic granitoids) in the Yagan MCC, showing mixing proportions between two end-members: (1) juvenile components (basalt), and (2) crustal components (the Precambrian basement gneisses): the core gneisses (host rocks of the granitoits) from the Yagan MCC and the Xilinhot gneisses. The parameters of the hypothetical basaltic rocks are: [Sr] = 300 (ppm), ^{87}Sr/^{86}Sr = 0.7043, [Nd] = 10 ppm, εNd(t) = +8. For data of the gneisses see Table 4. Xilinhot gneisses: [Sr] = 250 (ppm), ^{87}Sr/^{86}Sr = 0.715, [Nd] = 20 ppm, εNd (t) = -10 (the used age is 230 Ma, almost the same as that (228 Ma) of the early Mesozoic granitoids) (after Chen et al., 2000).

to be more robust and Sm/Nd ratios can be more accurately measured, relative to Sr, and they provide a much clearer and less ambiguous constrains to the origin of granitic rocks (Jahn et al., 2000a), the following discussions are mainly based on the Nd isotopic data.

6. Discussion

6.1. Source of the Mesozoic granitoids

The Mesozoic granitoids in the Yagan MCC show a high-K concentrations, and have εNd (t) values of -2 to $+5$. However, the host gneisses, the lower plate of the Yagan MCC, have a normal calc-alkali geochemical characteristics and very negative εNd (t) values of -11 (Table 4). They are a part of the Precambrian basement (Wang et al., 2001a) uplifted from the lower- or middle-crust to the present-day level by formation of the MCC, and could represent the composition of the middle (or lower) crust in the area (Wang, 2000). Therefore, the granitoids could not be derived from melting of the basement rocks at the middle- (or lower-) crust levels only. Additionally, the low crystallization fractionation of the early Mesozoic granitoids, shown by the mean negative abnormal of δEu and the low SiO$_2$, (mostly 55–64%) indicates that their alkaline and high-K features were not the result of fractionation. Therefore, the high-K and shoshonitic features are considered to be related to a contribution from the juvenile mantle, as suggested by the high (positive) εNd (t) values. Furthermore, the alkaline and high-K features require that the juvenile mantle-derived compositions were metasomatized shortly before the melting event. This could interprets both the their alkaline and high-K features and high (positive) εNd (t) values.

Generation of granitoids with high (positive) εNd (t) values could be achieved by several ways. They could be produced by melting of lower crust, newly underplated juvenile magma(s) in a subduction setting (e.g. Bryant et al., 1997). However, the high (positive)-εNd (t) value Mesozoic granitoids in the study area are mostly post-collisional, similar to the most post-collisional granitoids in the CAOB, such as in Xinjiang (Zhao et al., 1996; Han et al., 1997; Chen et al., 2000; Chen and Jahn, 2002), and NE China (Wu et al., 2000), so that their generation processes were more complicated (Jahn et al., 2000c). In this study, the occurrence of magmatic-textured enclaves, which are usually interpreted to be globules of a more mafic magma that mingled with the host while it was still partially liquid (e.g. Elburg, 1996), may be an evidence for magmatic mixing. They have slightly higher positive εNd (t) values ($+1.19$) and lower (^{87}Sr/^{86}Sr)i values than those of the two host-rock samples, although their εNd (t) values are lower than that ($+5$) of one host-rock sample. Equilibration between the enclaves and host rocks might have changed the mineralogy and (isotopic) geochemistry of the enclaves

(Elburg, 1996). Originally, the Sr and Nd isotopic compositions might have considerably more mantle-like than those of the host rocks. If so, magmatic mixing may have played a role in generation of the granitic magma.

From an Nd isotopic review, the sources of the granitoids could also be explained by interaction and mixing between continental components and juvenile mantle-derived components. The lower plate of the Yagan MCC could represent the end-member of the continental contribution. The other end member, the juvenile mantle-derived components, has not been well constrained. If mantle-derived basaltic rocks, which might have been underplated magma or melted from underplated lower crust, are assumed to represent it as some studies suggested (e.g. Chen et al., 2000; Wu et al., 2000), a simple mixing calculation could be made (Fig. 10). The results show that the data of the late Mesozoic granitoids can approximately be explained by simple mixing. The proportion of the basaltic component involved in the generation of the late Mesozoic granitoids reach 70–80%, or even 90%. The data of the early Mesozoic granitoids, however, could not be well confined. This may imply that there might have been another crustal component. If the Xilinhot gneisses (Xu et al., 1996; Chen et al., 2000), which is located in the same tectonic belt as the Yagan MCC (1800 km to east along the Solonker suture, Fig. 1), are used as a crustal component, their mixing with the end-member of the basalt could approximately explain the data of the early Mesozoic granitoids (Fig. 10). Slight less basaltic material (55–70%) was involved in the generation.

Regarding the few garnet-bearing peraluminous granites (A/NCK = 1.17) of the early Mesozoic granitoids, their Sr and Nd isotopic compositions are the nearly same as major (early) rocks of the early Mesozoic granitoids; thus they have same origin as the major rocks and can not be S-type granites derived from felsic crustal compositions. They are probably the late phase evolved from of the early Mesozoic granitoids.

6.2. Tecotonic setting and implications

6.2.1. Early Mesozoic magmatism and deep-crustal extension

The early Mesozoic granitoids in the Yagan MCC have similar potassic and shoshonitic features, and show post-collisional or post-orogenic extensional setting. Generally, potassic granitoids form during late- to post-orogenic transpression/extension and crustal uplift, and HKCA magmatism occurs typically in post-collisional settings (Liégeois et al., 1998). Their tectonic discriminations diagrams of the early Mesozoic granitoids also indicate this setting. More importantly, the granitoids experienced syn-emplacement extensional-shear deformation under conditions of magmatic flow to high- and middle-temperature deformation, as mentioned above. All these suggest that adjustment, thinning and extension at middle-low crustal levels probably started during their emplacement (228 Ma).

In addition, synchronous A-type granites also occur 10 km to the south of the study area (228 Ma, zircon U–Pb, Wang et al., 1998), and early Mesozoic mafic intrusions, dikes and A-type granites also occur in northern China such as the Da Hinggan Mountains (Shao and Zhao, 1998), which is about 3000 km to the east of the study area, but within the CAOB (Fig. 1). These consistently indicate extension in the early Mesozoic. This setting for the origin of the early Mesozoic granitoids could be explained by a model of convective thinning or removal of lithosphere beneath mountain belts and concomitant rise of hot asthenosphere (Turner et al., 1996; Väisänen et al., 2000).

The study in this area is concerned with the problem of the timing of collision between the Altaid belt and north China orogenic belt (Manchurides) along the Solonker suture. Some authors proposed that the collision took place in the Permo-Triassic (Sengör et al., 1993; Wang and Liou, 1986; Ruzhentsev et al., 1989). This is recently supported by recognition of subduction-related granitoids (310 Ma) and syn-collisional granites (230 Ma) (Chen et al., 2000). On other hand, others argued for suturing in the middle Devonian to early Carboniferous (Tang, 1990; Xu and Chen, 1997; Shao, 1991; Hong et al., 1995). Our present age data suggest that an extensional tectonic regime at least started at 228 Ma in the Yagan area. Additionally, the last regional compressional deformations structures (folds and cleavages) under conditions of low greenschist facies metamorphism were cut by a 263 ± 2 Ma (zircon U–Pb) pluton (Wang, 2000). This indicates that the regional compressional deformation, which could correspond to a late Paleozoic collisional orogeny along the suture, must have taken place before 263 Ma. Consequently, we suggest that the final collision and suturing was completed before 263 Ma. The early Mesozoic magmatism in the Yagan area probably occurred in a post-orogenic (or even intraplate) setting if the collision took place in the middle Devonian to early Carboniferous, or in a post-collisional setting if the collision took place in the early Permian.

It is interesting that the middle-late Jurassic Mesozoic great thrust also occurs in the study area (Zheng et al., 1991, 1996). Its relationships to the early and late Mesozoic extension need further studies.

6.2.2. Late Mesozoic magmatism and extension caused by uplift

The original relationship between granitic magmatism and extension, as in MCCs, has long been a subject of controversy (Leeman and Harry, 1993; Lister and Baldwin, 1993). The following relations enable us to conclude that the late Mesozoic magmatism caused and accelerated the final formation of the MCC. First, the determination of age of 135 ± 2 Ma implies that the granitic plutons were emplaced during the extension of the MCC, because the extensional deformation continued from 170 to 120 Ma, and their emplacement was synchronous with rapid uplift of the MCC, as indicated by the rapid cooling history of the Hure

pluton (Wang, 2000). Second, the plutons were forcefully emplaced, and this could provide a driving force for the uplift (Wang et al., 2002). Third, the emplacement of the voluminous granitoids with mantle-derived components not only added to the volume of the core, resulting in its expansion, but also deduced the density of the core, and so increased its buoyancy. This also demonstrates that the addition of juvenile mantle-derived components provided ideal conditions for the formation of the Yagan MCC.

In general, post-collisional magmatism is mainly potassic and in particular high-K calc-alkaline with subordinate amounts of shoshonitic rocks, and shoshonitic magmatism often postdates the high-K calc-alkaline magmatism (Liégeois et al., 1998). In this region, however, the early Mesozoic magmatism with shoshonitic characteristics predated the late, high-K, calc-alkaline magmatism. Thus, these may belong to two separated magmatic systems. The early Mesozoic granitoids might be a result of Paleozoic post-collisional or post-orogenic magmatism, marking the end of Paleozoic magmatism. In contrast, the late Mesozoic granitoids may be different type of post-orogenic or intraplate magmatism linked to late Mesozoic extension. If so, the late Mesozoic extension may mark the start of a new tectonic extensional cycle, not related to Paleozoic post-orogeny.

6.3. Implications for crustal growth

The Mesozoic granitoids in the study area also have high (near positive) εNd (t) values (-2 to $+5$). Such isotope characteristics are different from those (with negative εNd (t) values) from other orogenic belts in the world, such as the Caledonian (e.g. Frost and O'Nions, 1985; Dempsey et al., 1990; Skjerlie, 1992) and Hercynian Belts (e.g. Liew and Hofmann, 1988; Ajaji et al., 1998; Azevedo and Nolan, 1998) in western Europe, but largely compatible with the general scenario for much of the Phanerozoic post-collision granitoids in the Central Asian Orogenic Belt (CAOB, e.g. Jahn et al., 2000a,b,c,d), such as in NE China (Wu et al., 2000), northern Xinjiang (Han et al., 1997; Hu et al., 2000; Chen et al., 2000; Chen and Jahn, 2002), Inner Mongolia (Hong et al., 1995, 1996; Chen et al., 2000), Kazakhstan (Heinhorst et al., 2000) and Mongolia and Transbaikalia (Kovalenko et al., 1996; Wickham et al., 1996; Litvinovsky et al., 1994; Zanvilevich et al., 1995; Litvinovsky and Zanvilevich, 1998). The generation of these massive granitoids suggests a significant addition of mantle material (juvenile component) to the continental crust, and implies considerably continental growth (Jahn et al., 2000a,b,c,d). Our study presents an additional example to reinforce this point.

Compared with the most granitoids (with εNd (t) values of 0 and $+8$) of the CAOB (e.g. Jahn et al., 2000c), the granitoids in the study area have slightly lower εNd (t) values and larger variation of the model ages (0.6–2.2 Ga). This may be due to the influence of an old continent,
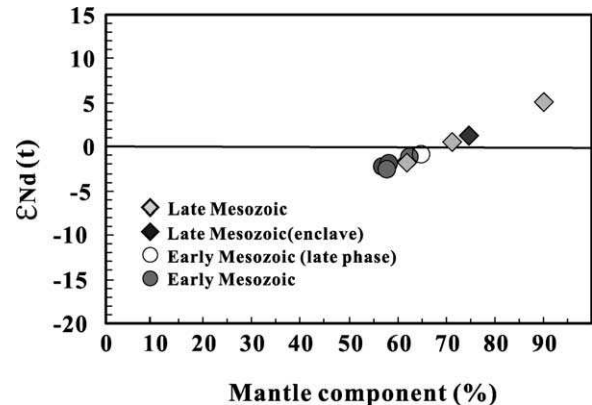

Fig. 11. Estimate of the proportion of the mantle or juvenile component in the generation of the granitoids of the Yagan MCC. The equation used is: $X^m = (\varepsilon^c - \varepsilon^r)$ Nd$^c/(\varepsilon^r(Nd_m - Nd^c) - (\varepsilon^m Nd_m - \varepsilon^c Nd^c))$, where X^m = % mantle component (represented by basalt; $\varepsilon^c, \varepsilon^r, \varepsilon^m$ = Nd isotopic composition of the crustal component, rock measured, and mantle component, respectively; Nd$_c$, Nd$_m^c$ = Nd concentrations in the crustal and mantle components, respectively. After Jahn et al., 2000c. For parameters see Fig. 10.

the Proterozoic south Mongolian microcontinent (Wang et al., 2001a). However, they have slightly higher εNd (t) values than granitoids from other old microcontinents in the CAOB, such as the Jiamusi Massif in NE China (Wu et al., 2000). These suggest that more juvenile mantle-derived components were involved in the formation of the granitoids in the study area. Juvenile mantle-derived components involved in the generation of granitoids mean that they contributed to the growth of the continental crust (Jahn et al., 2000b,c,d). If a simple mixing equation of Nd isotopes is used to estimate the juvenile component (Fig. 11), the generation of the early Mesozoic granitoids will need involvement of 57–64% of a basaltic component, and the late Mesozoic granitoids will require a slightly greater amount of basaltic material (61–74% , or even 90%). Interestingly, both the volume and involved juvenile mantle-derived components of the late Mesozoic granitoids are greater than those of the early Mesozoic granitoids (e.g. Fig. 11). Thus, the volume of crustal growth appears to be in direct proportion to the extension intensity, because the late Mesozoic extension (the main phase of the formation of the MCC) was stronger than the early Mesozoic extension.

All these suggest that the three processes, magmatism, extension and vertical continental growth, are closely related, which are all probably related to the intensity of interaction between crust and mantle at deep levels, i.e. addition of mantle-derived components (such as underplating) and delamination of the lower crust.

7. Conclusions

1. The intrusive granitoids in the Yagan–Onch Hayrhan MCC near the Mongolian border in China were once regarded as Paleozoic magmatic rocks. New

geochronological data indicate that they were emplaced in early and late Mesozoic times. The early Mesozoic granitoids are dated at 228 ± 7 Ma, and rich in alkaline. They were emplaced in post-collisional setting, and experienced extensional syn-tectonic magmatic flow and high-temperature solid flow. The late Mesozoic granitoids, dated at 135 ± 2 Ma, have high-K calc-alkaline characteristics. They were forcefully emplaced in a post-orogenic or intraplate extensional setting, and accelerated the final formation of the MCC.

2. Both the early and late Mesozoic granitoids have εNd (t) values of -2 to $+5$, highly distinguished from the value of -11 for their host gneisses from middle (or lower) crust and suggest that juvenile mantle-derived components have participated in the generation of the magmas. These features are largely compatible with the general scenario for much of the Phanerozoic post-collision granitoids in the Central Asian Orogenic Belt, which provide evidence for Phanerozoic continental growth.

3. The study shows that tectonic extension, magmatism and crustal growth are closely related, and that post-collisional, post-orogenic or even intraplate magmatism was probably a significant process of continental growth in the Phanerozoic.

Appendix A. Analytical methods

After carefully identified, the representative samples were analyzed. Major element contents were analyzed by wet chemistry, and rare earth and other trace element abundances were determined by XRF (3080, made in Japan) and for some low content elements by ICP-AES and ICP-AES-MS (JA1160, produced by company TJA POEMS, USA) at the Laboratory Center, Institute of Geology, Chinese Academy of Geological Sciences, Beijing. Analytical precision is less than $0.5-1\%$ for major element oxides and less than $5-10\%$ for rare earth and other trace element abundances. Accuracy was controlled by analyses of Chinese standards.

Nd–Sr isotopes were analyzed by isotope dilution at the Isotope Laboratory, Institute of Geology, Chinese Academy of Geological Sciences, Beijing (samples No. 1–6) and the Laboratory Center, Institute of Geology, Chinese Academy of Geological Sciences (No. 7–10). Analytical procedures were after Qiao (1988) and Huang and Wu (1990), and Zhang et al. (1994). Results of international reference samples analyzed in these laboratories agree manually within analytical uncertainties. Rb, Sr, Sm and Nd concentrations were obtained by isotope dilution; a mixed ^{87}Rb–^{84}Sr–^{149}Sm–^{150}Nd spike solution was used. Isotopic ratio measurements were made on a multicollector VG-354 thermal ionization mass spectrometer, described by Qiao (1988). All measured ^{87}Sr/^{86}Sr and ^{143}Nd/^{144}Nd ratios were normalized to ^{86}Sr/^{88}Sr 0.119400 and ^{146}Nd/^{144}Nd 0.721900, respectively. The mean of the measured ^{143}Nd/^{144}Nd of the La Jolla Nd standard was 0.511863 ± 7 (2σ, $n = 6$). Errors are quoted throughout as two standard deviations from measured or calculated values. Analytical uncertainties are estimated to be $<0.5\%$ for both ^{87}Rb/^{86}Sr and ^{147}Sm/^{147}Nd ratios. The decay constants used in the εNd (t) calculations are λ^{87}Rb $= 1.42 \times 10^{-11}$/yr and λ^{147}Sm $= 6.54 \times 10^{-12}$/yr. Nd isotopic compositions are reported in normal εNd notation (DePaolo, 1988) using present-day values of 0.512638 for ^{143}Nd/^{144}Nd and 0.1966 for ^{147}Sm/^{144}Nd in CHUR. Nd model ages were calculated for present-day values of 0.513151 for ^{143}Nd/^{144}Nd and 0.21357 for ^{147}Sm/^{144}Nd, which corresponds to a linear increase from εNd (4.55 Ga) $= 0$ to εNd (0) $= +10$.

U–Pb zircon isotopic analyses of the late Mesozoic granitoids (sample 69/1) were made at the Tianjin Institute of Geology and Mineral Resources, China Geological Survey. The analytical methods and processes were described in detail by Li et al. (1995). Fist-size samples were crushed to less than 200 Am, and mineral separations were undertaken after elutriation. Approximately 30 grains of zircon were handpicked from each sample and homogeneous zircons with no inclusions or fissures were chosen for isotopic analyses. Dissolution of zircon and U, Pb chemical separation followed the procedures of Krogh (1973, 1982) with slight modification. ^{205}Pb/^{235}U spike was added to zircon samples in a 0.25 ml fluorine-plastic capsule for zircon dissolution. The final isolated U and Pb were loaded on an Re filament with silica gel–phosphoric acid. Mass analyses were carried out on a VG 354 mass spectrometer with Daly collector. All the U and Pb data were corrected for mass fractionation. The blanks were $0.03-0.05$ ng for Pb, and $0.002-0.004$ ng for U. Decay constants used in age calculation were ^{238}U $= 0.155125 \times 10^{-9}$ and ^{235}U $= 0.98485 \times 10^{-9}$ year^{-1}.

U–Pb zircon isotopic analyses of the early Mesozoic granitoids (sample I13) were conducted in the laboratory of the Department of Geology, University of Arizona, Tucson,

Arizona, USA. The method and process were described in Gehrels (2000). All uncertainties are at the 95% confidence level. Uncertainties in isotope ratios are in percent. Uncertainties in ages are in millions of years. Most concentrations have an uncertainty of 25% due to uncertainty in weight of grain. Constants used: $^{238}U/^{235}U = 137.88$. Decay constant for $^{235}U = 9.8485 \times 10^{-10}$. Decay constant for $^{238}U = 1.55125 \times 10^{-10}$. Pb blank ranged from 2 to 10 pg. U blank was < 1 pg. All analyses conducted using conventional isotope dilution and thermal ionization mass spectrometry.

References

Ajaji, T., Weis, D., Giret, A., Bouabdellah, M., 1998. Coeval potassic and sodic calc-alkaline series in the post-collisional Hercynian Tanncherfi intrusive complex, northeastern Morocco: geochemical, isotopic and geochronological evidence. Lithos 45, 371–393.

Azevedo, M.R., Nolan, J., 1998. Hercynian late-post-tectonic granitic rocks from the Fornos de Algodres area (Northern Centralduring post-thickening collapse: Insights from a crustal cross section through a Variscan metamorphic core complex. Geology 23, 905–908.

Batchelor, R.A., Bowden, P., 1985. Petrogenetic interpretation of granitoid rock series using multication parameters. Chem. Geol. 48, 43–55.

Bryant, C.J., Arculus, R.J., Chappell, B.W., 1997. Clarence river supesuite: 250 Ma Cordilleran tonalitic I-type intrusions in eastern Australia. J. Petrol. 38, 975–1001.

Byamba, J., 1996. Tectonics of old structures and phosphates of Mongolia. Transaction 57, 12–52. (In Russian).

Chen, B., Jahn, B.M., Wile, S., Xu, B., 2000. Two contrasting Paleozoic magmatic belts in northern Inner Mongolia, China: petrogenesis and tectonic implications. Tectonophysics 328, 157–182.

Chen, B., Jahn, B.M., 2002. Geochemical and isotopic studies of the sedimentary and granitic rocks of the Altai Orogen of NW China and their tectonic implications. Geol. Mag. 139 (1), 1–13.

Chen, J.F., Zhou, T., Xie, Z., Zhang, X., Guo, X., 2000. Formation of positive εNd (t)granitoids from the Alataw Mountains, Xinjiang, China, by mixing and fractional crystallization: implication for Phanerozoic crustal growth. Tectonophysics 328, 53–67.

Dempsey, C.S., Halliday, A.N., Meighan, I.G., 1990. Combined Sm–Nd and Rb–Sr isotope systematics in the Donegal granitoids and their petrogenic implications. Geol. Mag. 127, 75–80.

DePaolo, D.J., 1988. Neodymium Isotope Geochemistry: an Introduction, Springer, New York, p. 181.

Elburg, M.A., 1996. Evidence of isotopic equilibration between micro-granitoid enclaves and host granodiorite, Warburton Granodiorite, Lanchlan Fold Belt, Australia. Lithos 38, 1–22.

Frost, C.D., O'Nions, R.K., 1985. Caledonian magma genesis and crustal recycling. J. Petrol. 26, 515–544.

Gehrels, G.E., 2000. Reconnaissance geology and U–Pb geochronology of the western flank of the Coast Mountains between Juneau and Skagway, southeastern Alaska. In: Stowell, H.H., McClelland, W.C. (Eds.), Tectonics of the Coast Mountains, Southeast Alaska and Coastal British Columbia: Geological Society of America Special Paper, 342, pp. 213–234.

Graham, S.A., Hendrix, M.S., Badach, G., Badamgarav, D., 1996. Sedimentary record of transition from contractile to extensional tectonics, Mesozoic, southern Mongolia. GSA 28 (7), 68.

Han, B.F., Wang, S.G., Jahn, B.M., Hong, D.W., Kagami, H., Sun, Y.L., 1997. Depleted-mantle source for the Ulungur river A-type granites from north Xinjiang, China: geochemistry and Nd–Sr isotopic evidence, and implications for Phanerozoic crustal growth. Chem. Geol. 138, 135–159.

Heinhorst, J., Lehmann, B., Ermolov, P., Serykh, V., Zhurutin, S., 2000. Paleozoic crustal growth and metallogeny of Central Asia: evidence from magmatic–hydrothermal ore system of Central Kazakhstan. Tectonophysics 328, 69–87.

Hong, D.W., Huang, H.Z., Xiao, Y.J., Xu, H.M., Jin, M.Y., 1995. Permian alkaline granites in central inner Mongolia and their geodynamic significance. Acta Geol. Sinica 8, 27–39.

Hong, D.W., Wang, S.G., Han, B.F., Jin, M.Y., 1996. Post-orogenic alkaline granites from China and comparisons with anorogenic alkaline granites elsewhere. J. Southeast Asian Earth Sci. 13, 13–27.

Hu, A.Q., Jahn, B.M., Zhang, G.X., Chen, Y.B., Zhang, Q.F., 2000. Crustal evolution and Phanerozoic crustal growth in northern Xinjiang: Nd isotopic evidence: Part I. Isotopic characterization of basement rocks. Tectonophysics 328, 15–51.

Huang, X., Wu, L.R., 1990. Nd–Sr isotopes of granitoids from Shanxi Province and their significance for tectonic evolution. Acta Petrol. Sinica 6, 1–11. (in Chinese with English abstract).

Jahn, B.M., Wu, F.Y., Chen, B., 2000a. Granitoids of the Central Asian orogenic Belt and continental growth in the phanerozoic transaction of the Royal Society of Edinburgh. Earth Sci. 91, 181–193.

Jahn, B.M., Griffin, W.L., Windley, B.F., 2000b. Continental growth in the phanerozoic: evidence from Central Asia special issue. Tectonophysics 328 (1–2), 1–227.

Jahn, B.M., Wu, F.Y., Hong, D.W., 2000c. Massive granitoids generation in Central Asia: Nd isotopic evidence and implication for continental growth in the Phanerozoic. Episodes 23 (2), 82–92.

Jahn, B.M., Wu, F.Y., Hong, D.W., 2000d. Important crustal growth in the phanerozoic: isotopic evidence of granitoids from East central Asia. Proc. Indian Acad. Sci. (Earth Planet Sci.) 109, 5–20.

Johnson, C.L., Graham, S.A., Webb, L.E., Badarch, G., Beck, M., Hendrix, M.S., Lenegen, R., Sjostrom, D., 1997. Sedimentary response to late Mesozoic extension, southern Mongolia. Eos (Transactions, American Geophysical Union) 78, F175.

Krogh, T.E., 1973. A low-contamination method for hydrothermal decomposition of zircon and extractions of U and Pb for isotopic age determinations. Geochim. Cosmochim. Acta 37, 485–494.

Krogh, T.E., 1982. Improved accuracy of U–Pb zircon dating by the creation of more concordant systems using air abrasion technique. Geochim. Cosmochim. Acta 46, 637–649.

Kovalenko, V.I., Yarmolyuk, V.V., Kovach, V.P., Kotov, A.B., Kozakov, I.K., Sal'nikova, E.B., 1996. Sources of Phanerozoic granitoids in Central Asia: Sm–Nd isotope data. Geochem. Int. 34, 628–640.

Küster, D., Harms, U., 1998. Post-collisional potassic granitoids from the southern and northwestern parts of the Late Neoproterozoic East African Orogen: a review. Lithos 45, 177–195.

Leeman, W., Harry, D.L., 1993. A binary source model for extension-related magmatism in the Great Basin, western North America. Science 262, 1550–1554.

Litvinovsky, B.A., Zanvilevich, A.N., Wickham, S.M., 1994. The Angara–Vitim Batholith Transbaikalia: structure, petrology and petrogenesis. Geol. Geofiz. 7–8, 218–234.

Litvinovsky, B.A., Zanvilevich, A.N., 1998. Compositional trends of silicic and mafic magmas formed in the course of evolution of the Mongolian–Transbaikalian mobile belt. Russ. Geol. Geophys. 39, 155–180.

Li, H.M., Dong, S.W., Xu, J.S., 1995. Singe zircon U–Pb dating of gabbros from Quanzhou: origin of basic magma in east Fujian province, China. Chin. Sci. Bull. 40, 158–160. (in Chinese).

Liégeois, J.P., Navez, L., Hertogen, J., Black, R., 1998. Contrasting origin of post-collisional high-K calc-alkaline and shoshonitic versus alkaline peralkaline granitoids. The use of sliding normalization. Lithos 45, 1–28.

Lister, G.S., Baldwin, S.L., 1993. Plutonism and the origin of the metamorphic core complex. Geology 21, 607–610.

Liew, T.C., Hofmann, A.W., 1988. Precambrian crustal components, plutonic assimilations, plate environment of the Hercynian fold belt of central Europe: indications from Nd and Sr isotopic study. Contrib. Mineral. Petrol. 98, 129–138.

Maniar, P.D., Piccoli, P.M., 1989. Tectonic discrimination of granitoids. Geol. Soc. Am. Bull. 101, 635–643.

Ningxia Bureau of Geology, 1982. Geological map of the Haribuge area (K-48-X X) at a scale of 1:200,000 and the geologic report, People's Republic of China.

Pearce, J.A., 1982. Trace element characteristics of lavas from destructive plate boundaries. In: Thorpe, R.S., (Ed.), Andestites, Wiley, New York, pp. 525–548.

Pearce, J.A., Harris, N.B.W., Tindle, A.G., 1984. Trace element discrimination diagrams for the tectonic interpretation of granitic rocks. J. Petrol. 25, 956–983.

Pearce, J.A., 1996. Sources and settings of granitic rocks. Episodes 19, 120–125.

Peccerillo, R., Taylor, S.R., 1976. Geochemistry of Eocene calc-alkaline volcanic rocks from the Kastamoin area, northern Turkey. Contrib. Mineral. Petrol. 25, 956–983.

Qiao, G.S., 1988. Normalization of isotopic dilution analysis: a new program for isotope mass spectrometric analysis. Scientia Sinica, Ser. A 31, 1263–1268.

Ritts, B.D., Darby, B.J., Cope, T., 2001. Early Jurassic extensional basin formation in the Daqing Shan segment of the Yinshan belt, northern North China Block, Inner Mongolia. Tectonophysics 339, 239–258.

Ruzhentsev, S.V., Pospelov, I.I., Badarch, G., 1989. Tectonics of the Indosinides of Mongolia. Geotectonics 6, 13–27.

Sengör, A.M.C., Natal'in, B.A., Burtman, V.S., 1993. Evolution of the Altaid tectonic collage and Paleozoic crustal growth in Eurasia. Nature 364, 299–307.

Sengör, A.M.C., Natal'in, B.A., 1996. Paleotectonics of Asia: fragments of a synthesis. In: Yin, A., Harrison, T.M. (Eds.), The Tectonic Evolution of Asia, Cambridge University Press, Cambridge, pp. 486–641.

Shao, J.A., 1991. Crustal Evolution in the Middle Part of the Northern Margin of the Sino–Korean Plate, Peking University, Publishing House, Beijing, China (in Chinese with English abstract).

Shao, J.A., Zhao, G.L., 1998. Mesozoic tectonic evolution in the south part of Da Hinggan Mountains, northeastern China. Sci. China 28 (3), 193–200.

Skjerlie, K.P., 1992. Petrogenesis and significance of late Caledonian granitoid magmatism in western Norway. Contrib. Mineral. Petrol. 110, 473–487.

Sun, S.S., McDonough, W.F., 1989. Chemical and isotopic systematics of oceanic basalts: implications for mantle composition and processes. In: Saunder, A.D., Norry, M.J. (Eds.), Magmatism in the Ocean Basins, Geological Society Special Publication No. 42, pp. 313–345.

Tang, K.D., 1990. Tectonic development of Paleozoic fold belts at the northern margin of the Sino–Korean craton. Tectonics 9, 249–260.

Tribe, I.R., D'lemos, R.S., 1996. Significance of a hiatus in down-temperature fabric development within syn-tectonic quartz diorite complexes, Channel Islands, UK. J. Geol. Soc. London 153, 127–138.

Turner, S., Arnaud, N., Liu, J., Rogers, N., Hawkesworth, C., Harris, N., Kelley, S., Van Calsteren, P., Deng, W., 1996. Post-collision, shoshonitic volcanism on the Tibetan Plateau: implications for convective thinning of the lithosphere and the source of ocean island basalts. J. Petrol. 37, 45–71.

Väisänen, M., Mänttäri, I., Kriegsman, L.M., Holttä, P., 2000. Tectonic setting of post-collisional magmatism in the Palaeoproterozoic Svecofennian Orogen, SW Finland. Lithos 54, 63–81.

Whalen, J.B., Currie, K.L., Chappell, B.W., 1987. A-type granites: geochemical characteristics, discrimination and petrogenesis. Contrib. Mineral. Petrol. 95, 407–419.

Wang, Q., Liou, X.Y., 1986. Paleoplate tectonics between Cathaysia and Angaraland in Inner Mongolia of China. Tectonics 5, 1073–1088.

Wang, T., 2000. Mechanism, process and dynamics of the formation of the Yagan metamorphic core complex, Sino–Mongolian border area: major evidence from the generation, evolution and deformation of the granitoid plutons. Postdoctoral thesis of Peking University, pp. 1–40 (in Chinese with English abstract).

Wang, T., Wang, X.X., Li, W.P., 2000. Evaluation of multiple emplacement mechanisms of the Huichizi pluton, the Qinling orogenic belt, central China. J. Struct. Geol. 22, 505–518.

Wang, T., Zheng, Y.D., Gehrels, G.E., Mu, Z.G., 2001a. Geochronological evidence for existence of the south Mongolian microcontinent: a zircon U–Pb age of granitoid gneisses from the Yagan–Onch Hayrhan metamorphic core complex on the Sino–Mongolian border. Chin. Sci. Bull. 46, 2005–2008.

Wang, T., Zheng, Y.D., Li, T.B., Ma, M.B., Gao, Y.J., 2001b. Structures of mylonitic granitoid plutons of the Yagan metamorphic core complex in the Sino–Mongolian boundary area—constraint for the kinematics and chronology of the MCC. Prog. Nat. Sci. 11 (10), 766–771.

Wang, T., Zheng, Y.D., Li, T.B., 2002. Forceful emplacement of granitic plutons in an extensional tectonic setting: syn-kinematic plutons in the Yagan–Onch Hayrhan metamorphic core complex on the Sino–Mongolian border. Acta Geol. Sinica 76 (1), 81–88.

Wang, T.Y., Gao, J., Wang, J., 1998. Magmatism of a collisional and post-orogenic period in the northern Alaxa region in Inner Mongolia. Acta Geol. Sinica 72 (2), 126–137 (in Chinese with English abstract).

Webb, L.E., Graham, S.A., Johnson, C.L., Badarch, G., Beck, M., Hendrix, M.S., 1997. Characteristics and implications of the Onch Hayrhan metamorphic core complex of southern Mongolia. Eos (Transactions American Geophysical Union) 78, 174–175.

Webb, L.E., Graham, S.A., Johnson, C.L., Badarch, G., Hendrix, M.S., 1999. Occurrence, age, and implication of the Yagan–Onch Hayrhan metamorphic core complex, southern Mongolia. Geology 27 (2), 143–146.

Wickham, S.M., Albert, A.D., Zanvilevich, A.N., Litvnovsky, B.A., Bindeman, I.N., Schuble, E.A., 1996. A stable isotope study of anorogenic magmatism in East Central Asia. J. Petrol. 37, 1063–1095.

Wu, F.Y., Jahn, B.M., Wilde, S., Sun, D.Y., 2000. Phanerozoic crustal growth: U–Pb and Sr–Nd isotopic evidence from granites in northeastern China. Tectonophysics 328, 89–113.

Xu, B., Chen, B., 1997. The structure and evolution of a Middle-Paleozoic orogenic belt between the North China and Siberian Blocks, northern Inner Mongolia, China. Sci. China Ser. D 27 (3), 227–232 (in Chinese with English abstract).

Xu, B., Chen, B., Shao, J.A., 1996. Sm–Nd and Rb–Sr isotopic geochronology of the Xilinhot Complex, Inner Mongolia. Chin. Sci. Bull. 41, 1107–1110.

Yanshin, A.L., 1989. Map of geological formations of the Mongolian People's Republic, Academica Nauka USSR, Moscow, 2 sheets, scale 1:1500,000.

Zanvilevich, A.N., Litvinovsky, B.A., Wickham, S.M., Bea, F., 1995. Petrogenesis of the Kharitonovo plutonic alkaline complex, South Transbaikalia, Russia. J. Petrol. 103, 127–145.

Zhang, Z.Q., Liu, D.Y., Fu, G.M., 1994. Study of the chronology of Qinling metamorphic stratigraphy, Geological Publishing House, Beijing (in Chinese with English abstract).

Zhao, Z.H., Wang, Z.G., Zou, T.R., Masuda, A., 1996. Study on petrogenesis of alkali-rich intrusive rocks of Ulungur, Xinjiang. Geochemica 25 (3), 205–220 (in Chinese with English abstract).

Zheng, Y.D., Wang, S., Wang, Y., 1991. An enormous thrust nappe and extensional metamorphic core complex newly discovered in the Sino–Mongolian boundary area. Sci. China (ser. B) 34 (9), 1146–1152.

Zheng, Y.D., Zhang, Q., 1994. The Yagan metamorphic core complex and extensional detachment fault in Inner Mongolia. Acta Geologica Sinica 7 (2), 125–135.

Zheng, Y.D., Zhang, Q., Wang, Y., Liu, R., Zuo, G., Wang, S., Lkaasuren, B., Badarch, G., Badamgarac, Z., 1996. Great Jurassic thrust sheets in Beishan (North Mountains)–Gobi areas of China and southern Mongolia. J. Struct. Geol. 18, 1111–1126.

Zheng, Y.D., Wang, T., Ma, M.B., Davise, G.A., 2003. Maximum effective moment criterion and the origin of low-angle normal faults. J. Struct. Geol. in press.